Separation of the valley exciton-polariton in two-dimensional semiconductors with an anisotropic photonic crystal

Ruoming Peng,[1] Changming Wu,[1] Huan Li,[1] Xiaodong Xu,[2,3] and Mo Li[1,2,*]

[1]*Department of Electrical and Computer Engineering, University of Washington, Seattle, Washington 98195, USA*

[2]*Department of Physics, University of Washington, Seattle, Washington 98195, USA*

[3]*Department of Material Science and Engineering, University of Washington, Seattle, Washington 98195, USA*

(Received 26 March 2020; revised manuscript received 17 May 2020; accepted 20 May 2020; published 15 June 2020)

Excitons in two-dimensional (2D) transition metal dichalcogenides (TMDC) are stable at room temperature because of high exciton binding energies. They can be selectively addressed based on the unique optical selection rules from angular momentum conservation for the K/K valley state and the helicity of circularly polarized light. When coupled with the optical modes in optical cavities, excitons can form exciton-polaritons, exploiting which in 2D TMDC may lead to optoelectronic devices for room temperature operation. The valley degree of freedom of the excitons, however, is mostly lost when forming exciton-polaritons because the cavity mode usually does not have a well-defined spin angular momentum. Here, we theoretically demonstrate that the valley information of exciton-polaritons can be preserved and resolved in a photonic cavity made of birefringent materials. Because of the optical anisotropy, the guided resonance modes have a net transverse spin angular momentum and selectively couple to exciton-polaritons with the corresponding valley state. In the strong-coupling regime, the exciton-polariton behaves in a way like the Rashba effect in the solid. The dispersion of the K/K exciton-polariton splits in momentum space based on its valley state, similar to electron spins in Rashba systems. Realizing valley-dependent exciton-polaritons affords a possibility to explore valley exciton dynamics in a strongly coupled system and will contribute to the study of excitonic, polaritonic devices, Bose-Einstein condensation, and superfluidity in semiconductors.

DOI: 10.1103/PhysRevB.101.245418

I. INTRODUCTION

Two-dimensional (2D) transition metal dichalcogenides (TMDCs), such as MoS_2 and WSe_2, have shown the potential in enabling the next generation of optoelectronic devices such as nanolaser, photodetector, and nonlinear optic elements [1–11]. With improved sample quality, 2D TMDC and their heterostructures have shown high photoluminescence quantum yields, long exciton lifetime, large nonlinear optical coefficients, and efficient electro-optic tunability [5,6,8,12–16]. Thanks to the reduced screening effects at the monolayer limit, exciton binding energy can reach several hundred meV [7,13,17,18], orders of magnitude higher than that in conventional semiconductors such as GaAs or InGaAs [19–21]. The large exciton binding energy makes it possible to realize stable exciton-polariton and Bose-Einstein condensation (BEC) in these 2D materials at room temperature [15,16,22–28]. Furthermore, the hexagonal lattice structure with broken inversion symmetry gives rise to the valley degree of freedom (d.o.f.) [29–33], which can be selectively addressed with circularly polarized light. TMDCs have integrated with photonic cavities to enhance the light-matter interaction to reach the strong coupling regime in which exciton-polaritons are formed. Because exciton-polaritons have ultrastrong nonlinearity, photon-like coherence, and excitonic interactions [19–21,34], they present a prototypical model system for studying quantum optical phenomena, many-body physics (e.g., BEC), and developing low-threshold nanolasers [4,19,20,34] and a chip-based quantum simulator [35,36].

Exciton-polaritons in TMDCs have been observed in a variety of photonic systems such as plasmonic cavities [16,18,23,24,37,38], distributed Bragg reflector (DBR) cavities [18,25,26], and guided resonance of photonic crystals [39]. To address the valley states optically, light needs to be circularly polarized, which is difficult to achieve in photonic devices. Spatially resolving the valley states would facilitate their control, readout, and interfacing with other photonic devices. It was recently realized that the evanescent field of spatially confined quasitransverse modes (TE or TM) in photonic devices are circularly polarized in the plane of propagation. The evanescent field thus carries a spin angular momentum that is transverse to the propagation. Exploiting this transverse spin angular momentum (tSAM) of light in various photonic devices has led to chiral light-matter interaction in many material systems such as quantum dots, topological insulators, and TMDCs [40–48].

However, because most of the photonic structures possess mirror symmetry, the tSAM is highly localized such that its spatial average over the whole surface around the photonic device will vanish. The tSAM $\boldsymbol{S}$ of the photonic structure is

*moli96@uw.edu

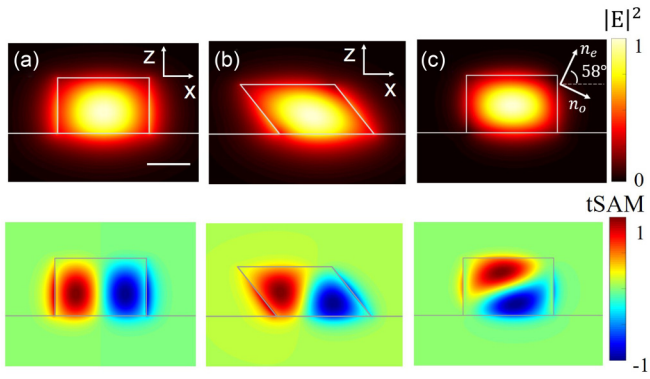

FIG. 1. Calculated fundamental mode profile (upper panel) and tSAM distribution (lower panel) for different waveguide geometry, the scale bar is 200 nm. (a) Mode profile and tSAM for the rectangular SiN_x waveguide on SiO_2 substrates. The net transverse tSAM (S_z) on the waveguide top is canceled due to the mirror symmetry of the waveguide. (b) SiN_x waveguide structure by angled etching technique, the symmetry breaking in the waveguide shape induce the nonzero tSAM on the waveguide top. (c) The (101) rutile waveguide on the sapphire substrate. Rutile is anisotropic by introducing the birefringence of the materials, the rutile rectangular waveguide results in the finite net tSAM on the waveguide top surface.

defined as $\boldsymbol{S} = \mathrm{Im}(\epsilon_0 \boldsymbol{E}^* \times \boldsymbol{E} + \mu_0 \boldsymbol{H}^* \times \boldsymbol{H})/4\omega$ [43,49,50]. In the SAM definition, $\boldsymbol{E}$ and $\boldsymbol{B}$ are the electric and magnetic field, ϵ_0 and μ_0 are the vacuum permittivity and permeability, and ω is the angular frequency. For example, although the fundamental mode of a rectangular waveguide carries nonzero tSAM in the z direction (S_z) locally as shown in Fig. 1(a), its distribution is an odd function of the x coordinate, leading to a zero net tSAM on the top surface of the waveguide. Therefore, the averaged effect of light-matter interaction with a layer of material on top of the waveguide will show no chirality, or valley selectivity in the case of TMDCs. This observation can be generalized to any photonic systems with mirror symmetry.

To enable valley selective optical interaction, it is necessary to break the mirror symmetry. For example, if the TMDCs on top of the waveguide is made asymmetric, chiral interaction could be achieved [51]. Similarly, if the rectangular waveguide is made angled, as shown in Fig. 1(b), the net tSAM on the top surface will not vanish. Etching the waveguide with angled sidewalls, however, will be rather challenging. Other than geometric asymmetry, the intrinsic birefringence of a material can also break the mirror symmetry to achieve a finite net tSAM in a photonic device. Here, we consider rutile, the crystalline TiO_2. The ratio of its refractive index along extraordinary and ordinary optical axes (n_e/n_o) about 1.12, which is among the highest values of natural materials. Rutile can be epitaxially grown with (101) crystalline orientation on sapphire substrates by molecular beam epitaxy [52]. The (101) orientation causes the extraordinary axis to be tilted at an angle of 32 from the out-of-plane direction. Photonic devices made of such an anisotropic material with tilted optical axis will have broken mirror symmetry. Take the simple rectangular waveguide for an example as shown in Fig. 1(c), the tSAM on its top surface does not change sign with the x coordinate, which results in a nonvanishing net total tSAM, similar to the situation of an angled waveguide.

II. RESULTS AND DISCUSSIONS

Integrating TMDCs with photonic devices made of optically anisotropic materials will make it possible to address and control the valley d.o.f. in TMDCs through chiral optical interactions. Recently, the exciton-polariton state was observed at room temperature in monolayer WSe_2 integrated on a one-dimensional (1D) photonic crystal in which excitons are strongly coupled with the guided resonance [39]. Because the photonic structure is made of isotropic material silicon nitride (SiN_x), excitons of different valleys cannot be discriminated in this system. Inspired by this work and the above consideration, we consider replacing SiN_x with an anisotropic material, such as (101) rutile on the sapphire substrate, to make an anisotropic photonic crystal. The birefringence of rutile breaks the mirror symmetry of the photonic crystal and makes the optical coupling chiral, which will enable control of the valley state of the exciton-polaritons.

The coordinate of the studied system is defined in Fig. 2(a). The extraordinary optical axis of the rutile film is titled in the x-z plane so mirror symmetry around y axis is broken. We only need to consider the dispersion relation with respect to the wave vector k_y direction as the guided resonance mode carries tSAM pointed along the z axis. By tuning of the period, filling factor, total thickness and etched depth of the 1D photonic crystal (period Λ: 330 nm, filling factor η: 0.88, total thickness t: 160 nm, etch depth h: 89 nm), we engineer the energy of the mode of interest to be close to the WSe_2 exciton energy (1.73 eV). The numerically simulated mode profile at $k_y = -5\ \mu m^{-1}$, and the corresponding tSAM $\boldsymbol{S}$ distribution, are plotted in in Figs. 2(b) and 2(c). Compared to the SiN_x device, as plotted in Fig. 2(d), the integral of $\boldsymbol{S}$ on the top surface in the rutile device is no longer zero, which will lead to chiral coupling with circularly polarized excitation light. We define the degree of circular polarization p, the average of the local polarization over the top surface of the photonic crystal, for a specific mode by using Stokes parameters as

$$p = \frac{\int S_3 dA}{\int S_0 dA} = \frac{\int 2E_x E_y \sin(\delta) dA}{\int E_x^2 + E_y^2 dA}, \tag{1}$$

where A is the whole area of the top surface, S_0 and S_3 are Stokes parameters, $\delta = \delta_x - \delta_y$ denotes the phase difference between E_x and E_y components. We evaluate p at $k_y = -5\ \mu m^{-1}$ to be 0.5, which quantifies the chirality of the mode,the intensity of the left circular polarized (LCP) component is about three times the right circular polarized (RCP) component.

The chirality of this anisotropic photonic crystal can be experimentally investigated by measuring its reflection spectrum for incident light with a given circular polarization. The k-space dispersion of the reflection spectra can be calculated by scanning both the incident angle and frequency in numerical simulation. The sharper resonance of the reflection spectrum suggests more coupling to the guided resonance mode of the photonic crystal [53,54]. Figure 3(a) displays the calculated result for the rutile photonic crystal with LCP incident light and confirm its chiral response. It shows an

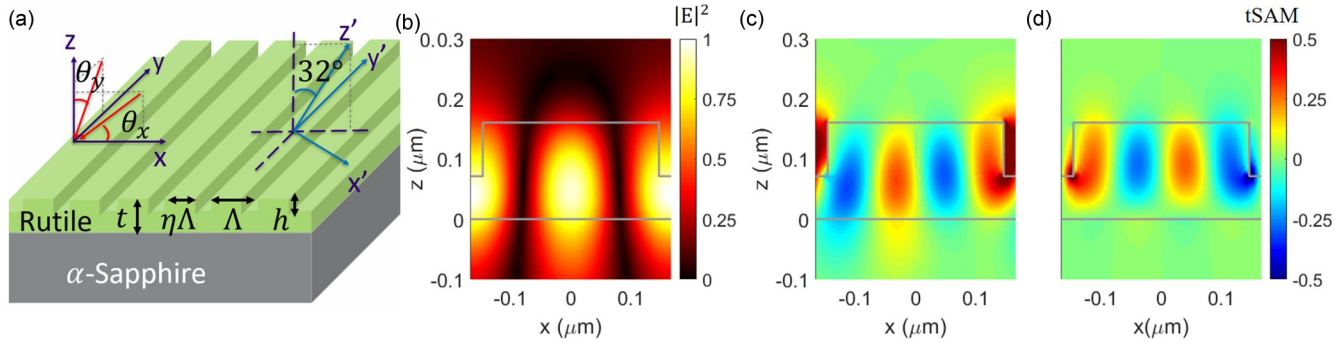

FIG. 2. The guided resonance mode of 1D photonic crystal. (a) The axis definition of the (101) rutile 1D photonic crystal and birefringence axis is shown in the figures. The n_e axis of (101) rutile has a tilting angle about 32 degrees. (b) The electric field profile for the specific resonance mode at $k_y = 0$. (c) The calculated tSAM for (101) rutile photonic crystal at $k_y = -5\ \mu m^{-1}$, the birefringence contributes to nonvanishing tSAM on the photonic crystal top surface. For $k_y = 5\ \mu m^{-1}$, tSAM with opposite sign is observed, which is preserved by the time reversal symmetry. (d) The calculated tSAM for the SiN_x photonic crystal at $k_y = -5\ \mu m^{-1}$, the net tSAM is zero.

asymmetric spectrum with respect to the incident angle-higher reflection at negative incident angles ($k_y < 0$) with sharper resonance than at positive angles ($k_y > 0$), which indicates a stronger coupling when $k_y < 0$. We also calculate the mode profile for each k_y and extract the quality factor and degree of polarization p of the guided resonance mode. This photonic crystal has decent quality factors of 240 over a wide range of k_y [Fig. 3(b)] with a linewidth in photon energy of γ_{pc}. The polarization p at different k_y is plotted in Fig. 3(c), showing that at negative (positive) k_y, the mode is more left-hand (right-hand) polarized.

The valley selection rule in TMDC dictates that the excitons of one valley (K or K) couple selectively with circularly polarized light of one helicity (left or right-handed). Here, we define the convention that the K valley only interacts with LCP light, whereas the K valley only interacts with RCP light. Consequently, the guided resonance modes at $k_y < 0$, which are LCP polarized, will have a stronger coupling with the K valley excitons, and vice versa for $k_y > 0$ modes and K valley excitons. When the coupling is sufficiently strong, exciton-polaritons will form. As the coupling strength overwhelms the loss, the exciton and photonic structures are considered strongly coupled such that the k-space dispersion will show avoided crossings due to Rabi splitting and form upper and lower branches in dispersion given by [21]

$$E_{\pm} = \frac{1}{2}(E_{exc} + E_{pc} + i(\gamma_{exc} + \gamma_{pc})/2) \pm \sqrt{g(k)^2 + \frac{1}{4}[E_{exc} - E_{pc} + i(\gamma_{exc} - \gamma_{pc})]^2}, \quad (2)$$

where E_{exc} and E_{pc} denote the exciton and photonic crystal resonance energy, γ_{exc} and γ_{pc} represent their linewidths, $g(k)$ is the coupling coefficient at a given k. We denote g_0 as the coupling coefficient when $k_y = 0$. The corresponding Rabi splitting for the polariton system is:

$$2\hbar\omega = \sqrt{g(k)^2 - \frac{1}{4}(\gamma_{exc} - \gamma_{pc})^2} \quad (3)$$

In order to resolve the splitting and observe the anti-crossing behavior in the system, the splitting $\hbar\omega$ should be larger than the total linewidth of the polariton system $(\gamma_{exc} + \gamma_{pc})/2$. The criteria of strong coupling for the exciton-polariton system is defined as

$$g(k) > \sqrt{\frac{1}{2}(\gamma_{exc}^2 + \gamma_{pc}^2)}. \quad (4)$$

As mentioned above, the coupling coefficient $g(k)$ between the exciton of a specific valley state with optical modes of

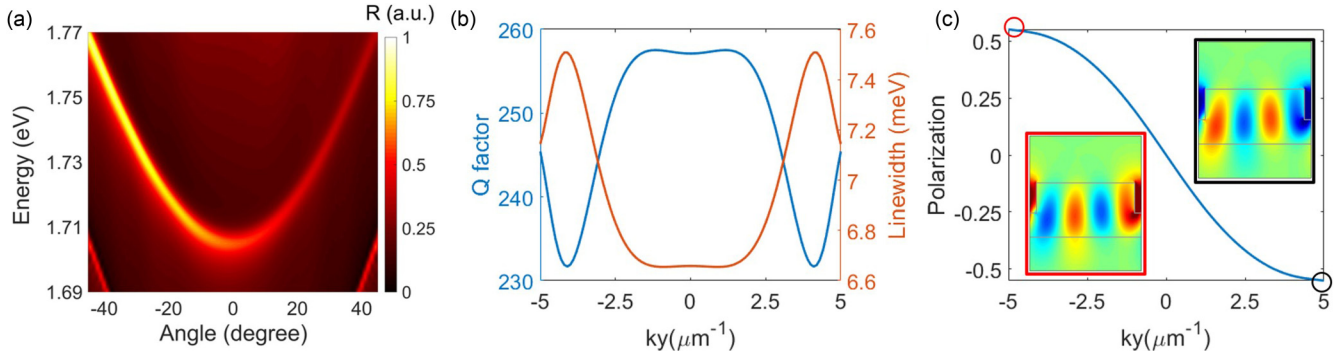

FIG. 3. Helicity dependent interactions in (101) Rutile 1D photonic crystals. (a) Reflection spectrum for the RCP light. We observe more reflection in the positive k_y side, which indicates stronger coupling between RCP light with guided resonance mode. (b) Calculated polarization for each k_y point. For $k_y = -5\ \mu m^{-1}$, polarization more than 0.5 could be achieved. (c) Calculated linewidth or quality factor for the resonance mode at each k_y. This would be used for calculating the condition of strong coupling regime.

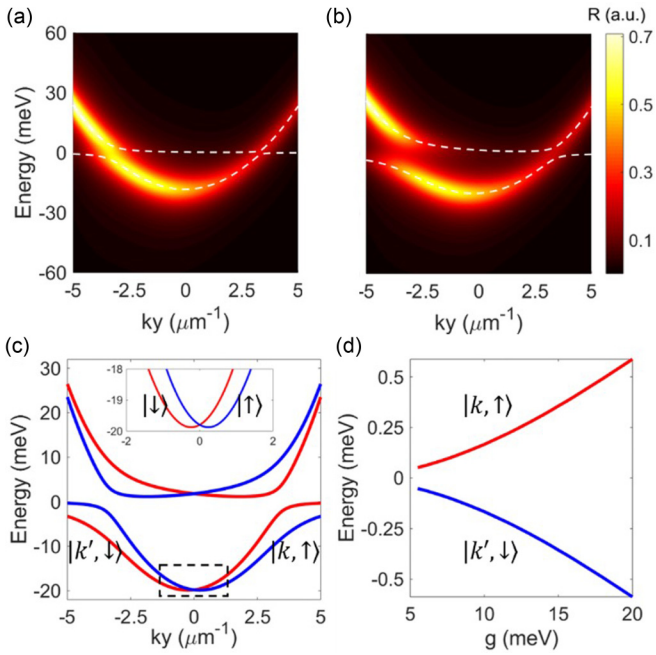

FIG. 4. Asymmetric momentum splitting in the exciton polariton dispersion. (a) The asymmetric splitting for $g = 5$ meV when we consider exciton polariton in the K valley. The obvious anticrossing behavior is observed in positive k_y side which is the signature of strong coupling regime, while there is no anticrossing behavior for the positive k_y side. The coupling strength is related to the polarization of the resonance mode where polarization for the positive k_y side is much smaller than the negative k_y side and less interaction would be expected. (b) For larger $g = 12$ meV, both positive and negative k_y show the anticrossing behaviors, but the Rabi splitting for these two k_y would be different. (c) Consider the lower branch of exciton polariton at large coupling strength g, the k_y for minimum energy is not zero. Inset: the zoom-in feature of the dashed region. Considering the K valley, the momentum for minimum energy would be the opposite. This splitting for different valley exciton polariton in momentum space is analogous to the Rashba effect in solid-state physics. (d) From the Hamiltonian of our polariton system, the splitting of the valley exciton polariton is the function of coupling strength. With increasing coupling strength, more splitting could be observed where the valley information could be perfectly extracted by taking into consideration of particular valley polariton dispersion.

different k_y are different. For K valley excitons, there exist a range of negative k_y where $g(k)$ is large enough to meet the strong-coupling requirement, but not for positive k_y. Figure 4(a) plots the calculated reflection spectrum when setting $g_0 = 5$ meV in the simulation. The linewidth of the exciton γ_{exc} is 5.7 meV at 10 K according to the measured results [39]. It is evident that anticrossing behavior is only observed on the negative k_y side of the dispersion. For positive k_y, however, because of insufficient coupling, anticrossing behavior does not appear.

If the coupling strength is increased further, both positive and negative k_y can reach the strong coupling regime. As shown in Fig. 4(b), when $g_0 = 12$ meV, both sides of k_y show anticrossing behaviors. Comparing the energy splitting of two different directions, the negative k_y direction still has a larger energy splitting, which corresponds to the larger coupling coefficient on the negative k_y side than the positive k_y side. To understand the physical behaviors of this strongly coupled system, its Hamiltonian can be written as [21]

$$H = E_{exc} b^\dagger b + E_{pc} a^\dagger a + g(k)(a^\dagger b + c.c.); \tag{5}$$

$$g(k) = \frac{g_0}{2}\left[1 + \mathrm{Im}\left(\frac{\int (\boldsymbol{E_x} \times \boldsymbol{E_y}) \cdot \boldsymbol{\sigma_z} dA}{\int E_x^2 + E_y^2 dA}\right)\right], \tag{6}$$

where $a^\dagger$ and $b^\dagger$ are the photon and exciton creation operators, the $g(k)$ term is related to net tSAM (polarization) and should be a function of k_y and $\sigma_z = \pm 1$ that is corresponding to the valley spin polarization. From the Hamiltonian, the interaction term $g(k)$ in the polariton system has a form $(\boldsymbol{E_x} \times \boldsymbol{E_y}) \cdot \boldsymbol{\sigma_z}$, which is similar to that for the Rashba spin-orbit coupling (SOC) term in a solid-state system when SOC is considered for 2D quantum well structures under a vertical electric field [55]. The Rashba SOC term could be written as $H_R = \alpha(\boldsymbol{E} \times \boldsymbol{P}) \cdot \boldsymbol{\sigma}$, where α is the Rashba coupling, $\boldsymbol{E}$ is the applied field, $\boldsymbol{P}$ is the momentum, and $\boldsymbol{\sigma}$ is the Pauli matrix. The breaking of the crystal symmetry in the z direction by the vertical field results in splitting of in-plane spins in the k space. By the same token, in the exciton-polariton system, the breaking of the 1D photonic crystal symmetry in the x direction by the crystalline anisotropy of the rutile results in the splitting of different valley exciton-polariton in the k space. Such analogy is evident from the similarity of the Hamiltonians of the two systems. Compared to the conventional Rashba effect, which is enabled by the k-dependent spin-orbit interaction, the mechanism of valley polariton splitting is the k-dependent interaction between photon tSAM and valley exciton pseudospin. As a result, the splitting of lower and upper polariton branches is confirmed in Fig. 4(c) where the different valley (K and K) exciton-polaritons have finite splitting in the k space. By the same token, in the exciton-polariton system, the breaking of the 1D photonic crystal symmetry in the x direction by the crystalline anisotropy of rutile results in the splitting of different valley exciton-polaritons in the k space. Such an analogy is evident from the similarity of the Hamiltonians of the two systems. Compared to the conventional Rashba effect, which is enabled by the k-dependent spin-orbit interaction, the mechanism of valley polariton splitting is the k-dependent interaction between photon tSAM and valley exciton pseudospin. As a result, the splitting of lower and upper polariton branches is confirmed in Fig. 4(c) where the different valley (K and K) exciton-polaritons have finite splitting in the k space. The splitting of valley polariton in the k space increases with increasing g_0, because stronger coupling results in a more significant difference between different valley polaritons. This is also confirmed by our calculations as shown in Fig. 4(d), which indicates that the splitting of valley polariton in k space is proportional to the coupling coefficient. Such splitting has interesting implications under the BEC condition, where all the polaritons will condensate at the lowest energy points so that the exciton-polariton with opposite valley information will condensate at different k points, and the valley information can be fully distinguished and extracted from the directional luminescent emission of the condensation.

III. CONCLUSION

In conclusion, we conceptualize the manipulation of 2D valley exciton polarization by engineering anisotropic photonic crystal structures with nonzero net tSAM on the top surface. We illustrate this concept with 1D photonic crystal structure made of a birefringent (101) rutile. When TMDC materials are integrated on the top of photonic crystal, valley polarized excitons with opposite spins will couple differently to modes with opposite k_y directions. We found that when strong-coupling is reached, the splitting of different valley polaritons in the k space is analogous to the Rashba spin orbit coupling effect. By taking advantage of material's optical anisotropy, the valley information of exciton-polariton in TMDC can be distinguished in the k space. This result can be generalized to 2D and 3D conditions, so the net tSAM is still preserved due to the mirror symmetry breaking induced by the material anisotropy. Given the limitation of zero tSAM interaction in photonic structures of isotropic materials, the anisotropic photonic crystal offers a platform to study valley exciton-polaritons in the TMDC thin film. From the technological perspective, the study of this anisotropic photonic system will benefit the development of functional optoelectronics and photonics devices. Also, utilization and manipulation of the valley exciton-polariton have great potential in chiral quantum optics and provide a degree of freedom for exploring future photonic structures.

ACKNOWLEDGMENTS

This work was supported by the National Science Foundation (NSF Award No. EFMA 1741656 and NSF MRSEC 1719797) and the Office of Naval Research (ONR) through a MURI Grant No. N00014-17-1-2661.

[1] B. Radisavljevic, A. Radenovic, J. Brivio, V. Giacometti, and A. Kis, Single-layer MoS_2 transistors, Nat. Nanotechnol. **6**, 147 (2011).

[2] S. Wu, S. Buckley, J. R. Schaibley, L. Feng, J. Yan, D. G. Mandrus, F. Hatami, W. Yao, J. Vučković, A. Majumdar, and X. Xu, Monolayer semiconductor nanocavity lasers with ultralow thresholds, Nature (London) **520**, 69 (2015).

[3] Y. Ye, Z. J. Wong, X. Lu, X. Ni, H. Zhu, X. Chen, Y. Wang, and X. Zhang, Monolayer excitonic laser, Nat. Photonics **9**, 733 (2015).

[4] C. Schneider, A. Rahimi-Iman, N. Y. Kim *et al.*, An electrically pumped polariton laser, Nature **497**, 348 (2013).

[5] D. Kufer and G. Konstantatos, Highly sensitive, encapsulated MoS_2 photodetector with gate controllable gain and speed, Nano Lett. **15**, 7307 (2015).

[6] Y. K. Srivastava, A. Chaturvedi, M. Manjappa, A. Kumar, G. Dayal, C. Kloc, and R. Singh, MoS_2 for ultrafast all-optical switching and modulation of THz Fano metaphotonic devices, Adv. Opt. Mater. **5**, 1700762 (2017).

[7] Y. Q. Bie, G. Grosso, M. Heuck, M. M. Furchi, Y. Cao, J. Zheng, D. Bunandar, E. Navarro-Moratalla, L. Zhou, D. K. Efetov, T. Taniguchi, K. Watanabe, J. Kong, D. Englund, and P. Jarillo-Herrero, A $MoTe_2$-based light-emitting diode and photodetector for silicon photonic integrated circuits, Nat. Nanotechnol. **12**, 1124 (2017).

[8] I. Datta, S. H. Chae, G. R. Bhatt, M. A. Tadayon, B. Li, Y. Yu, C. Park, J. Park, L. Cao, D. N. Basov, J. Hone, and M. Lipson, Low-loss composite photonic platform based on 2D semiconductor monolayers, Nat. Photon. **14**, 256 (2020).

[9] C. H. Liu, J. Zheng, S. Colburn, T. K. Fryett, Y. Chen, X. Xu, and A. Majumdar, Ultrathin van der Waals metalenses, Nano Letters **18**, 6961 (2018).

[10] H. Liu, Y. Li, Y. S. You, S. Ghimire, T. F. Heinz, and D. A. Reis, High-harmonic generation from an atomically thin semiconductor, Nat. Phys. **13**, 262 (2017).

[11] T. K. Fryett, K. L. Seyler, J. Zheng, C.-H. Liu, X. Xu, and A. Majumdar, Silicon photonic crystal cavity enhanced second-harmonic generation from monolayer WSe_2, 2D Mater. **4**, 015031 (2016).

[12] H. Zeng, J. Dai, W. Yao, D. Xiao, and X. Cui, Valley polarization in MoS_2 monolayers by optical pumping, Nat. Nanotechnol. **7**, 490 (2012).

[13] A. M. Jones, H. Yu, N. J. Ghimire, S. Wu, G. Aivazian, J. S. Ross, B. Zhao, J. Yan, D. G. Mandrus, D. Xiao, W. Yao, and X. Xu, Optical generation of excitonic valley coherence in monolayer WSe_2, Nat. Nanotechnol. **8**, 634 (2013).

[14] K. L. Seyler, J. R. Schaibley, P. Gong, P. Rivera, A. M. Jones, S. Wu, J. Yan, D. G. Mandrus, W. Yao, and X. Xu, Electrical control of second-harmonic generation in a WSe_2 monolayer transistor, Nat. Nanotechnol. **10**, 407 (2015).

[15] J. Shi, W.-Y. Liang, S. S. Raja, Y. Sang, X.-Q. Zhang, C.-A. Chen, Y. Wang, X. Yang, Y.-H. Lee, H. Ahn, and S. Gwo, Plasmonic enhancement and manipulation of optical nonlinearity in monolayer tungsten disulfide, Laser Photon. Rev. **12**, 1800188 (2018).

[16] J. Cuadra, D. G. Baranov, M. Wersäll, R. Verre, T. J. Antosiewicz, and T. Shegai, Observation of Tunable Charged Exciton Polaritons in Hybrid Monolayer WS_2-Plasmonic Nanoantenna System, Nano Lett. **18**, 1777 (2018).

[17] C. Robert, D. Lagarde, F. Cadiz, G. Wang, B. Lassagne, T. Amand, A. Balocchi, P. Renucci, S. Tongay, B. Urbaszek, and X. Marie, Exciton radiative lifetime in transition metal dichalcogenide monolayers, Phys. Rev. B **93**, 205423 (2016).

[18] N. Lundt, S. Klembt, E. Cherotchenko, S. Betzold, O. Iff, A. V. Nalitov, M. Klaas, C. P. Dietrich, A. V. Kavokin, S. Höfling, and C. Schneider, Room-temperature Tamm-plasmon exciton-polaritons with a WSe_2 monolayer, Nat. Commun. **7**, 13328 (2016).

[19] A. Imamoglu, R. J. Ram, S. Pau, and Y. Yamamoto, Nonequilibrium condensates and lasers without inversion: Exciton-polariton lasers, Phys. Rev. A **53**, 4250 (1996).

[20] H. Deng, G. Weihs, C. Santori, J. Bloch, and Y. Yamamoto, Condensation of semiconductor microcavity exciton polaritons, Science **298**, 199 (2002).

[21] H. Deng, H. Haug, and Y. Yamamoto, Exciton-polariton Bose-Einstein condensation, Rev. Mod. Phys. **82**, 1489 (2010).

[22] F. Barachati, A. Fieramosca, S. Hafezian, J. Gu, B. Chakraborty, D. Ballarini, L. Martinu, V. Menon, D. Sanvitto,

and S. Kéna-Cohen, Interacting polariton fluids in a monolayer of tungsten disulfide, Nat. Nanotechnol. **13**, 906 (2018).

[23] W. Liu, Y. Wang, B. Zheng, M. Hwang, Z. Ji, G. Liu, Z. Li, V. J. Sorger, A. Pan, and R. Agarwal, Observation and active control of a collective polariton mode and polaritonic band gap in few-layer WS_2 strongly coupled with plasmonic lattices, Nano Lett. **20**, 790 (2020).

[24] R. Liu, Z.-K. Zhou, Y.-C. Yu, T. Zhang, H. Wang, G. Liu, Y. Wei, H. Chen, and X.-H. Wang, Strong Light-Matter Interactions in Single Open Plasmonic Nanocavities at the Quantum Optics Limit, Phys. Rev. Lett. **118**, 237401 (2017).

[25] J. Gu, B. Chakraborty, M. Khatoniar, and V. M. Menon, A room-temperature polariton light-emitting diode based on monolayer WS_2, Nat. Nanotechnol. **14**, 1024 (2019).

[26] S. Dufferwiel, S. Schwarz, F. Withers, A. A. Trichet, F. Li, M. Sich, O. Del Pozo-Zamudio, C. Clark, A. Nalitov, D. D. Solnyshkov, G. Malpuech, K. S. Novoselov, J. M. Smith, M. S. Skolnick, D. N. Krizhanovskii, and A. I. Tartakovskii, Exciton-polaritons in van der Waals heterostructures embedded in tunable microcavities, Nat. Commun. **6**, 1 (2015).

[27] J. B. Khurgin, Two-dimensional exciton-polariton-light guiding by transition metal dichalcogenide monolayers, Optica **2**, 740 (2015).

[28] A. J. Leggett, Bose-Einstein condensation in the alkali gases: Some fundamental concepts, Rev. Mod. Phys. **73**, 307 (2001).

[29] J. Xiao, M. Zhao, Y. Wang, and X. Zhang, Excitons in atomically thin 2D semiconductors and their applications, Nanophotonics **6**, 1309 (2017).

[30] K. F. Mak and J. Shan, Photonics and optoelectronics of 2D semiconductor transition metal dichalcogenides, Nat. Photonics **10**, 216 (2016).

[31] P. Rivera, K. L. Seyler, H. Yu, J. R. Schaibley, J. Yan, D. G. Mandrus, W. Yao, and X. Xu, Valley-polarized exciton dynamics in a 2D semiconductor heterostructure, Science **351**, 688 (2016).

[32] D. Xiao, G. B. Liu, W. Feng, X. Xu, and W. Yao, Coupled Spin and Valley Physics in Monolayers of MoS_2 and Other Group-VI Dichalcogenides, Phys. Rev. Lett. **108**, 196802 (2012).

[33] H. Yu, X. Cui, X. Xu, and W. Yao, Valley excitons in two-dimensional semiconductors, Natl. Sci. Rev. **2**, 57 (2015).

[34] T. Byrnes, N. Y. Kim, and Y. Yamamoto, Exciton-polariton condensates, Nat. Phys. **10**, 803 (2014).

[35] I. Bloch, J. Dalibard, and S. Nascimbène, Quantum simulations with ultracold quantum gases, Nat. Phys. **8**, 267 (2012).

[36] N. Y. Kim and Y. Yamamoto, Exciton-polariton quantum simulators, in *Quantum Simulations with Photons and Polariton*, edited by D. Angelakis (Springer, Cham, 2017) pp. 91–121.

[37] W. Liu, B. Lee, C. H. Naylor, H. S. Ee, J. Park, A. T. Johnson, and R. Agarwal, Strong exciton-plasmon coupling in MoS_2 coupled with plasmonic lattice, Nano Lett. **16**, 1262 (2016).

[38] B. Lee, W. Liu, C. H. Naylor, J. Park, S. C. Malek, J. S. Berger, A. T. Johnson, and R. Agarwal, Electrical tuning of exciton-plasmon polariton coupling in monolayer MoS_2 integrated with plasmonic nanoantenna lattice, Nano Lett. **17**, 4541 (2017).

[39] L. Zhang, R. Gogna, W. Burg, E. Tutuc, and H. Deng, Photonic-crystal exciton-polaritons in monolayer semiconductors, Nat. Commun. **9**, 713 (2018).

[40] A. Aiello, N. Lindlein, C. Marquardt, and G. Leuchs, Transverse Angular Momentum and Geometric Spin Hall Effect of Light, Phys. Rev. Lett. **103**, 100401 (2009).

[41] X. Yin, Z. Ye, J. Rho, Y. Wang, and X. Zhang, Photonic Spin Hall Effect, Science **339**, 1405 (2013).

[42] J. Petersen, J. Volz, and A. Rauschenbeutel, Chiral nanophotonic waveguide interface based on spin-orbit interaction of light, Science **346**, 67 (2014).

[43] A. Aiello, P. Banzer, M. Neugebauer, and G. Leuchs, From transverse angular momentum to photonic wheels, Nat. Photonics **9**, 789 (2015).

[44] X. Ling, X. Zhou, X. Yi, W. Shu, Y. Liu, S. Chen, H. Luo, S. Wen, and D. Fan, Giant photonic spin Hall effect in momentum space in a structured metamaterial with spatially varying birefringence, Light: Sci. Appl. **4**, e290 (2015).

[45] K. Y. Bliokh, F. J. Rodríguez-Fortuño, F. Nori, and A. V. Zayats, Spin-orbit interactions of light, Nat. Photonics **9**, 796 (2015).

[46] K. Y. Bliokh, D. Smirnova, and F. Nori, Quantum spin Hall effect of light, Science **348**, 1448 (2015).

[47] S. Luo, L. He, and M. Li, Spin-momentum locked interaction between guided photons and surface electrons in topological insulators, Nat. Commun. **8**, 2141 (2017).

[48] I. S. Osborne, Nanoscale chiral valley-photon interface, Science **359**, 881 (2018).

[49] X. Ling, X. Zhou, K. Huang, Y. Liu, C. W. Qiu, H. Luo, and S. Wen, Recent advances in the spin Hall effect of light, Reports on Prog. Phys. **80**, 066401 (2017).

[50] W. Luo, S. Xiao, Q. He, S. Sun, and L. Zhou, Photonic spin Hall effect with nearly 100 efficiency, Adv. Opt. Mater. **3**, 1102 (2015).

[51] L. Sun, C. Y. Wang, A. Krasnok, J. Choi, J. Shi, J. S. Gomez-Diaz, A. Zepeda, S. Gwo, C. K. Shih, A. Alù, and X. Li, Separation of valley excitons in a MoS_2 monolayer using a subwavelength asymmetric groove array, Nat. Photonics **13**, 180 (2019).

[52] B. Jalan, R. Engel-Herbert, J. Cagnon, and S. Stemmer, Growth modes in metal-organic molecular beam epitaxy of TiO_2 on r-plane sapphire, J. Vac. Sci. Technol. A **27**, 230 (2009).

[53] B. P. Pal (Ed.), *Guided Wave Optical Components and Devices: Basics, Technology, and Applications* (Academic press, 2010).

[54] E. Waks and J. Vuckovic, Dipole Induced Transparency in Drop-Filter Cavity-Waveguide Systems, Phys. Rev. Lett. **96**, 153601 (2006).

[55] Y. A. Bychkov and E. I. Rashba, Oscillatory effects and the magnetic susceptibility of carriers in inversion layers, J. Phys. C **17**, 6039 (1984).